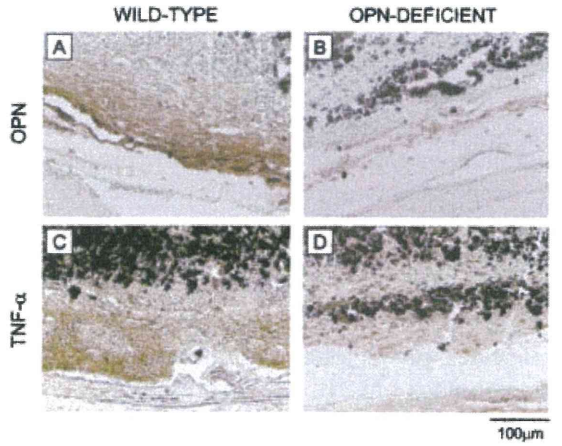

Figure 4. Expression of osteopontin (OPN) and tumor necrosis factor α (TNFα) in a murine calvaria resorption model. OPN protein expression in the membrane and bone surface of the bone resorption area was enhanced in wild-type (WT) animals (**A**) but was not detected in OPN$^{-/-}$ animals (**B**). TNFα expression in the membrane and bone surface of the bone resorption area was enhanced in WT animals (**C**), whereas it was hardly detected in OPN$^{-/-}$ animals (**D**). Color figure can be viewed in the online issue, which is available at http://www.arthritisrheum.org.

expressed in the membranous tissue and on the bone surface in the bone resorption area in WT mice (Figure 4A). No specific staining was seen in the membranous tissue or bone surface in OPN-deficient mice (Figure 4B), confirming the lack of OPN expression in these animals. TNFα, the inflammatory cytokine implicated in particle-induced osteolysis, was highly expressed in membranous tissue and on the bone surface in bone resorption areas in WT mice (Figure 4C), whereas TNFα expression was reduced in OPN-deficient mice (Figure 4D). These observations suggest that OPN may play a role in cytokine secretion from macrophages stimulated by wear particles.

Effect of OPN deficiency on cytokine secretion by BMMs in response to titanium particle treatment. To further investigate the effect of OPN deficiency in macrophages stimulated by particles, the secretion of TNFα and other osteolysis-associated cytokines was evaluated using cultured BMMs. FACS analysis indicated that ~70% of bone marrow stromal cells were differentiated into macrophages, and the number of CD11b-positive cells was similar in both genotypes (results not shown). The OPN concentration in the cell culture supernatants of BMMs from WT mice was significantly higher following exposure to titanium particles (Figure 5G). OPN was not detected in cell culture supernatants of OPN-deficient BMMs regardless of exposure to particles (data not shown).

TNFα levels were significantly lower in cell culture supernatants of BMMs from OPN-deficient mice as compared with BMMs from WT mice after exposure to titanium particles (Figure 5A). Furthermore, levels of the proinflammatory cytokines IL-1α, IL-1β, and IL-6 and the chemotactic factors MCP-1 and MIP-1α were significantly reduced in culture supernatants of BMMs from OPN-deficient mice (Figures 5B–F). In contrast, the secretion of IL-17 and RANTES was not affected by OPN deficiency (data not shown). These data indicate that OPN participates in particle-mediated osteoclastogenesis via orchestration of inflammatory cytokine secretion from BMMs.

Lack of effect of OPN deficiency on phagocytic activity of BMMs. To investigate the effect of OPN deficiency on BMM phagocytic activity, we analyzed latex bead phagocytosis in BMMs from WT and OPN-deficient mice. Flow cytometric analysis revealed that BMMs from OPN-deficient mice have a phagocytic capacity similar to that of BMMs from WT mice (Figures 6A–D). These results indicate that OPN does not act in the regulation of BMM phagocytosis, at least not in vitro.

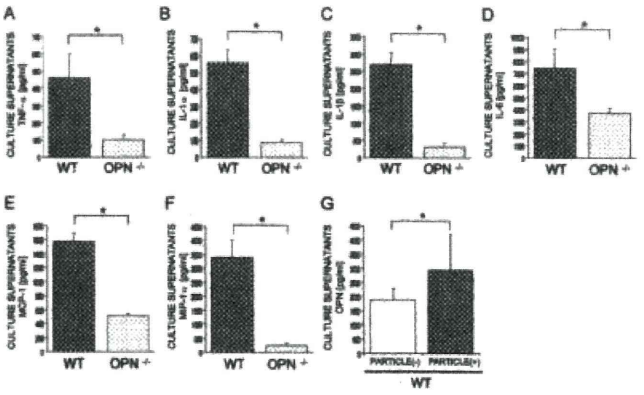

Figure 5. Osteolysis-associated cytokine concentrations in culture supernatants after exposure to titanium particles. Bone marrow–derived macrophages (BMMs) obtained from wild-type (WT) or osteopontin-deficient (OPN$^{-/-}$) mice were cultured with titanium particles for 12 hours. Concentrations of tumor necrosis factor α (TNFα) (**A**), interleukin-1α (IL-1α) (**B**), IL-1β (**C**), IL-6 (**D**), monocyte chemoattractant protein 1 (MCP-1) (**E**), and macrophage inflammatory protein 1α (MIP-1α) (**F**) in culture supernatants were determined. In addition, BMMs obtained from WT animals were cultured for 12 hours with or without titanium particles, and the OPN concentration in the culture supernatants was measured (**G**). Values are the mean and SEM. * = $P < 0.05$.

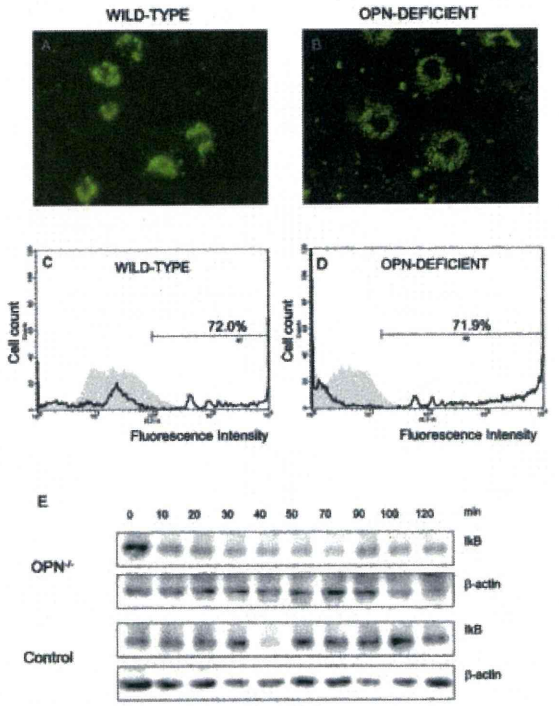

Figure 6. Phagocytic activity of bone marrow–derived macrophages (BMMs). **A** and **B,** BMMs obtained from the marrow of the long bones of wild-type (WT) and osteopontin-deficient ($OPN^{-/-}$) mice were exposed to fluorescence latex beads and incubated for 1 hour at 37°C (magnification × 400). **C** and **D,** The percentage of phagocytic macrophages in WT and $OPN^{-/-}$ mice was analyzed by flow cytometry. **E,** Impairment of phagocytosis-mediated IκB degradation in BMMs derived from $OPN^{-/-}$ mice. BMMs were isolated from 6-month-old $OPN^{-/-}$ mice and their WT control littermates. Cells were exposed to titanium particles for the indicated times. Transient IκB degradation, which causes NF-κB activation, was observed at 40 minutes after exposure in cells from control mice, while no obvious surge of IκB degradation was observed for up to 120 minutes in cells from $OPN^{-/-}$ mice. β-actin was used as a loading control. Color figure can be viewed in the online issue, which is available at http://www.arthritisrheum.org.

Phagocytosis-mediated IκB degradation in BMMs. To address the role of OPN on phagocytosis-mediated cytokine secretion, NF-κB activation was investigated in BMMs stimulated by titanium particles. BMMs from WT and OPN-deficient mice were exposed to titanium particles for various time periods (Figure 6E). Transient IκB degradation, which causes NF-κB activation, was clearly observed at 40 minutes after exposure in cells from control mice, while no obvious surge of IκB degradation was observed for up to 120 minutes in cells from OPN-deficient mice. Thus, phagocytosis-mediated NF-κB activation was impaired in BMMs from OPN-deficient mice.

DISCUSSION

The major cause of failure of long-term implants in patients with total joint replacements is aseptic loosening due to particle-induced osteolysis. A foreign-body, granulomatous response to material byproducts creates a chronic inflammatory reaction composed primarily of activated macrophages and fibroblasts. The periprosthetic tissues may produce high levels of proinflammatory cytokines (TNFα, IL-1, and IL-6, etc.), chemokines for macrophages, polymorphonuclear leukocytes and lymphocytes, prostanoids, and nitric oxide and superoxide metabolites (23,24). In the present study, we demonstrated that OPN is required for the progression of titanium particle–induced osteolysis in a murine calvaria model.

OPN protein and mRNA are expressed in macrophages in the periprosthetic tissue of patients with aseptically loosened prostheses (17). Here, we confirmed by ELISA elevated levels of OPN protein in the periprosthetic tissue. OPN is also expressed in human and murine granulomatous responses of diverse causes (15,16) and is required for functional granuloma formation (24). It is notable that OPN production is induced by a number of mediators that are abundantly expressed during cell-mediated/granulomatous inflammation (25). In particular, staining of TNFα was diminished in OPN-deficient animals, implicating OPN in the regulation of TNFα secretion in particle-induced osteolysis. TNFα, a potent cytokine produced by monocytes in response to titanium, is known to activate osteoclasts to resorb bone, and it has been shown to be critically involved in wear debris–induced osteolysis in vivo (5,22,26). TNFα also prompts osteoclastogenesis in cultured murine bone marrow (26). In this study, in vitro experiments with BMMs exposed to titanium particles indicated that OPN was indispensable for TNFα secretion by macrophages.

Decreased depth of bone resorption pits in OPN-deficient mice with particle-induced osteolysis suggested that OPN was indispensable for osteoclast function, as has been reported elsewhere (Figure 3). Osteoclasts express OPN, which stimulates bone resorption and osteoclast motility, thus increasing the number and depth of resorption pits (27). Osteoclasts from OPN-deficient mice are hypomotile and less active in bone resorption than are osteoclasts from WT mice. Thus, the function of secreted OPN as an osteoclast autocrine factor may be to stimulate cell motility and adhesion related to bone resorption. Since osteoclasts are actively migrating cells, hypomotility decreases bone resorption (27). Adhesion, organization for migration, and organi-

zation for resorption are sequential events that are necessary for osteoclast function (28), and OPN stimulates each of these events. Furthermore, an intracellular form of OPN that activates macrophages and metastatic cells through association with the CD44 complex (29) functions in the formation and activity of osteoclasts (30).

Phagocytic uptake involves actin dynamics, including polymerization, bundling, contraction, severing, and depolymerization of actin filaments. The Rho GTP binding proteins are signaling elements critical to the control of actin reorganization during a variety of phagocytic signaling processes (31,32). Osteoclasts stimulated with OPN were shown to recapitulate the effects of Rho and Cdc42 in phosphatidylinositol 4,5-bisphosphate association with Wiscott-Aldrich syndrome protein as well as actin ring formation (31,33,34). Thus, we speculated that OPN deficiency might affect the phagocytic activity of BMMs. However, the findings of our in vitro studies excluded this possibility (Figure 6) and indicated that the regulation of proinflammatory cytokines by OPN is independent of phagocytotic activity.

Our in vitro studies with BMMs from WT mice revealed increased OPN concentrations in culture supernatants after exposure to titanium particles. This result may be associated with the observation that OPN mRNA and protein expression from macrophages are enhanced by TNFα stimulation (35,36). Moreover, we confirmed that OPN protein expression levels were enhanced in human periprosthetic osteolysis tissues as compared with OA synovium. We speculate that the cytokine milieu produced by macrophages in particle-exposed synovium induces the overproduction of OPN. Our results also showed that levels of TNFα and other inflammatory cytokines (IL-1α, IL-1β, IL-6, MCP-1, and MIP-1α) were reduced in culture supernatants of cells from OPN-deficient mice via NF-κB inactivation, implicating OPN in the secretion of a variety of inflammatory cytokines by macrophages.

OPN activates the NF-κB transcription factor pathway, which is known to play a critical role in the production of many inflammatory cytokines and chemokines (37). NF-κB is the main factor involved in the transcription of MCP-1 and MIP-1α (38,39). Thus, inflammatory cytokine secretion is enhanced by OPN through NF-κB–mediated pathways. Overproduction of OPN, in turn, amplifies inflammation through proinflammatory chemokines and cytokines and promotes the migration and recruitment of inflammatory cells into the inflamed synovium (37). This mechanism, which is mediated by OPN, is likely to play a key role in periprosthetic osteolysis. Taken together, OPN and inflammatory cytokines may constitute a positive feedback loop in the periprosthetic soft tissues and may promote chronic inflammation.

We used titanium particles in this study. In the clinical setting, the most widely accepted implant configuration includes a metal component articulating against a polyethylene component (40). Today, total joint replacement with metal on ultrahigh molecular weight polyethylene is the international standard of care for degenerative joint disorders (40,41). Although it seems that polyethylene particles are the most common inducer of osteolysis around joint replacement implants (42), titanium particles have been commonly used for murine calvaria bone resorption models (5,22,40,42–44). Taki et al (44) recently reported that similar mechanisms were responsible for osteolysis induced by polyethylene and titanium particles.

Some current studies focused on the role of adherent endotoxin on titanium particles and particle-induced osteolysis (44–47). As reported by Ragab et al (45), it is unavoidable that substantial amounts of endotoxin adhere to the commercially available titanium particles even if the particles are sterilized. In addition, orthopedic implant surfaces contain significant levels of adherent endotoxin (45). Although the clinical relevance of adherent endotoxin in aseptic loosening is a subject of controversy, it increases the biologic effects of orthopedic wear particles in cell culture as well as in vivo (47). Tatro et al (46) demonstrated that systemically derived endotoxin accumulates when "endotoxin-free," commercially pure titanium particles are implanted on murine calvaria. This does not suggest that the wear particles are unimportant, but that they act together with endotoxin to induce osteolysis (46). Taken together, the balance between accumulation and clearance of endotoxin may regulate the rate of osteolysis in the murine calvaria model as well as in patients with aseptic loosening of a prosthesis (46).

Our findings provide evidence that in the absence of OPN, wear debris–induced osteolysis was impaired. From this standpoint, periprosthetic osteolysis might be blocked by reducing the function of OPN. Although we did not examine them in this study, OPN inhibitors, such as $\alpha v\beta 3$ antagonist and antibody against OPN, are promising agents for protecting against periprosthetic osteolysis. The use of TNFα antagonists to treat inflammatory diseases such as RA has dramatically increased in recent years, and a recent study demonstrated the effectiveness of TNFα inhibitors in the treatment of

aseptic loosening and wear debris–induced osteolysis (5). However, the enormous cost of this type of treatment restricts the use of such biologic drugs to a small number of selected patients with severe disease (19). Development of nonpeptide antagonists against OPN activity could solve such problems (19).

In conclusion, we have shown that OPN plays critical roles in wear debris–induced osteolysis. Our data suggest that OPN is a candidate for a therapeutic target in periprosthetic osteolysis.

ACKNOWLEDGMENTS

The authors would like to kindly thank Dr. Akimoto Nimura for assistance with the FACS analysis and Miyoko Ojima for expert help with the histologic analysis.

AUTHOR CONTRIBUTIONS

All authors were involved in drafting the article or revising it critically for important intellectual content, and all authors approved the final version to be published. Dr. Asou had full access to all of the data in the study and takes responsibility for the integrity of the data and the accuracy of the data analysis.

Study conception and design. Rittling, Okawa, Shinomiya, Muneta, Denhardt, Noda, Asou.

Acquisition of data. Shimizu, Okuda, Kato, Tsuji, Asou.

Analysis and interpretation of data. Shimizu, Okuda, Tsuji, Asou.

REFERENCES

1. Harris WH. Wear and periprosthetic osteolysis: the problem. Clin Orthop Relat Res 2001;393:66–70.
2. Jacobs JJ, Roebuck KA, Archibeck M, Hallab NJ, Glant TT. Osteolysis: basic science. Clin Orthop Relat Res 2001;393:71–7.
3. Willert HG. Reactions of the articular capsule to wear products of artificial joint prostheses. J Biomed Mater Res 1977;11:157–64.
4. Green TR, Fisher J, Stone M, Wroblewski BM, Ingham E. Polyethylene particles of a 'critical size' are necessary for the induction of cytokines by macrophages in vitro. Biomaterials 1998;19:2297–302.
5. Childs LM, Goater JJ, O'Keefe RJ, Schwarz EM. Effect of anti-tumor necrosis factor-α gene therapy on wear debris-induced osteolysis. J Bone Joint Surg Am 2001;83-A:1789–97.
6. Nakashima Y, Sun DH, Trindade MC, Chun LE, Song Y, Goodman SB, et al. Induction of macrophage C-C chemokine expression by titanium alloy and bone cement particles. J Bone Joint Surg Br 1999;81:155–62.
7. Shanbhag AS, Hasselman CT, Rubash HE. Inhibition of wear debris mediated osteolysis in a canine total hip arthroplasty model. Clin Orthop Relat Res 1997;344:33–43.
8. Granchi D, Verri E, Ciapetti G, Stea S, Savarino L, Sudanese A, et al. Bone-resorbing cytokines in serum of patients with aseptic loosening of hip prostheses. J Bone Joint Surg Br 1998;80:912–7.
9. Teitelbaum SL. Bone resorption by osteoclasts. Science 2000;289:1504–8.
10. Childs LM, Paschalis EP, Xing L, Dougall WC, Anderson D, Boskey AL, et al. In vivo RANK signaling blockade using the receptor activator of NF-κB:Fc effectively prevents and ameliorates wear debris-induced osteolysis via osteoclast depletion without inhibiting osteogenesis. J Bone Miner Res 2002;17:192–9.
11. Granchi D, Amato I, Battistelli L, Ciapetti G, Pagani S, Avnet S, et al. Molecular basis of osteoclastogenesis induced by osteoblasts exposed to wear particles. Biomaterials 2005;26:2371–9.
12. Denhardt DT, Noda M. Osteopontin expression and function: role in bone remodeling. J Cell Biochem Suppl 1998;30/31:92–102.
13. Denhardt DT, Noda M, O'Regan AW, Pavlin D, Berman JS. Osteopontin as a means to cope with environmental insults: regulation of inflammation, tissue remodeling, and cell survival. J Clin Invest 2001;107:1055–61.
14. Asou Y, Rittling SR, Yoshitake H, Tsuji K, Shinomiya K, Nifuji A, et al. Osteopontin facilitates angiogenesis, accumulation of osteoclasts, and resorption in ectopic bone. Endocrinology 2001;142:1325–32.
15. Saeki Y, Mima T, Ishii T, Ogata A, Kobayashi H, Ohshima S, et al. Enhanced production of osteopontin in multiple myeloma: clinical and pathogenic implications. Br J Haematol 2003;123:263–70.
16. Standal T, Hjorth-Hansen H, Rasmussen T, Dahl IM, Lenhoff S, Brenne AT, et al. Osteopontin is an adhesive factor for myeloma cells and is found in increased levels in plasma from patients with multiple myeloma. Haematologica 2004;89:174–82.
17. Zreiqat H, Kumar RK, Markovic B, Zicat B, Howlett CR. Macrophages at the skeletal tissue-device interface of loosened prosthetic devices express bone-related genes and their products. J Biomed Mater Res A 2003;65:109–17.
18. Yoshitake H, Rittling SR, Denhardt DT, Noda M. Osteopontin-deficient mice are resistant to ovariectomy-induced bone resorption. Proc Natl Acad Sci U S A 1999;96:8156–60.
19. Yumoto K, Ishijima M, Rittling SR, Tsuji K, Tsuchiya Y, Kon S, et al. Osteopontin deficiency protects joints against destruction in anti-type II collagen antibody-induced arthritis in mice. Proc Natl Acad Sci U S A 2002;99:4556–61.
20. Rittling SR, Denhardt DT. Osteopontin function in pathology: lessons from osteopontin-deficient mice. Exp Nephrol 1999;7:103–13.
21. Rittling SR, Matsumoto HN, McKee MD, Nanci A, An XR, Novick KE, et al. Mice lacking osteopontin show normal development and bone structure but display altered osteoclast formation in vitro. J Bone Miner Res 1998;13:1101–11.
22. Schwarz EM, Benz EB, Lu AP, Goater JJ, Mollano AV, Rosier RN, et al. Quantitative small-animal surrogate to evaluate drug efficacy in preventing wear debris-induced osteolysis. J Orthop Res 2000;18:849–55.
23. Goodman SB, Huie P, Song Y, Schurman D, Maloney W, Woolson S, et al. Cellular profile and cytokine production at prosthetic interfaces: study of tissues retrieved from revised hip and knee replacements. J Bone Joint Surg Br 1998;80:531–9.
24. Goodman SB, Trindade M, Ma T, Genovese M, Smith RL. Pharmacologic modulation of periprosthetic osteolysis. Clin Orthop Relat Res 2005;430:39–45.
25. O'Regan A, Berman JS. Osteopontin: a key cytokine in cell-mediated and granulomatous inflammation. Int J Exp Pathol 2000;81:373–90.
26. Merkel KD, Erdmann JM, McHugh KP, Abu-Amer Y, Ross FP, Teitelbaum SL. Tumor necrosis factor-α mediates orthopedic implant osteolysis. Am J Pathol 1999;154:203–10.
27. Chellaiah MA, Soga N, Swanson S, McAllister S, Alvarez U, Wang D, et al. Rho-A is critical for osteoclast podosome organization, motility, and bone resorption. J Biol Chem 2000;275:11993–2002.
28. Kanehisa J, Heersche JN. Osteoclastic bone resorption: in vitro analysis of the rate of resorption and migration of individual osteoclasts. Bone 1988;9:73–9.
29. Zohar R, Suzuki N, Suzuki K, Arora P, Glogauer M, McCulloch CA, et al. Intracellular osteopontin is an integral component of the CD44-ERM complex involved in cell migration. J Cell Physiol 2000;184:118–30.
30. Suzuki K, Zhu B, Rittling SR, Denhardt DT, Goldberg HA, McCulloch CA, et al. Colocalization of intracellular osteopontin

with CD44 is associated with migration, cell fusion, and resorption in osteoclasts. J Bone Miner Res 2002;17:1486–97.
31. Caron E, Hall A. Identification of two distinct mechanisms of phagocytosis controlled by different Rho GTPases. Science 1998; 282:1717–21.
32. Chellaiah MA. Regulation of actin ring formation by rho GTPases in osteoclasts. J Biol Chem 2005;280:32930–43.
33. Blanchoin L, Amann KJ, Higgs HN, Marchand JB, Kaiser DA, Pollard TD. Direct observation of dendritic actin filament networks nucleated by Arp2/3 complex and WASP/Scar proteins. Nature 2000;404:1007–11.
34. Cox D, Chang P, Zhang Q, Reddy PG, Bokoch GM, Greenberg S. Requirements for both Rac1 and Cdc42 in membrane ruffling and phagocytosis in leukocytes. J Exp Med 1997;186:1487–94.
35. Denhardt DT, Guo X. Osteopontin: a protein with diverse functions. FASEB J 1993;7:1475–82.
36. Patarca R, Saavedra RA, Cantor H. Molecular and cellular basis of genetic resistance to bacterial infection: the role of the early T-lymphocyte activation-1/osteopontin gene. Crit Rev Immunol 1993;13:225–46.
37. Xu G, Nie H, Li N, Zheng W, Zhang D, Feng G, et al. Role of osteopontin in amplification and perpetuation of rheumatoid synovitis. J Clin Invest 2005;115:1060–7.
38. Ueda A, Okuda K, Ohno S, Shirai A, Igarashi T, Matsunaga K, et al. NF-κB and Sp1 regulate transcription of the human monocyte chemoattractant protein-1 gene. J Immunol 1994;153:2052–63.
39. Grove M, Plumb M. C/EBP, NF-κB, and c-Ets family members and transcriptional regulation of the cell-specific and inducible macrophage inflammatory protein 1α immediate-early gene. Mol Cell Biol 1993;13:5276–89.
40. Von Knoch M, Jewison DE, Sibonga JD, Sprecher C, Morrey BF, Loer F, et al. The effectiveness of polyethylene versus titanium particles in inducing osteolysis in vivo. J Orthop Res 2004;22:237–43.
41. Kurtz SM, Muratoglu OK, Evans M, Edidin AA. Advances in the processing, sterilization, and crosslinking of ultra-high molecular weight polyethylene for total joint arthroplasty. Biomaterials 1999; 20:1659–88.
42. Ulrich-Vinther M, Carmody EE, Goater JJ, K Soballe, O'Keefe RJ, Schwarz EM. Recombinant adeno-associated virus-mediated osteoprotegerin gene therapy inhibits wear debris-induced osteolysis. J Bone Joint Surg Am 2002;84-A:1405–12.
43. Soloviev A, Schwarz EM, Darowish M, O'Keefe RJ. Sphingomyelinase mediates macrophage activation by titanium particles independent of phagocytosis: a role for free radicals, NFκB, and TNFα. J Orthop Res 2005;23:1258–65.
44. Taki N, Tatro JM, Nalepka JL, Togawa D, Goldberg VM, Rimnac CM, et al. Polyethylene and titanium particles induce osteolysis by similar, lymphocyte-independent, mechanisms. J Orthop Res 2005;23:376–83.
45. Ragab AA, Van De Motter R, Lavish SA, Goldberg VM, Ninomiya JT, Carlin CR, et al. Measurement and removal of adherent endotoxin from titanium particles and implant surfaces. J Orthop Res 1999;17:803–9.
46. Tatro JM, Taki N, Islam AS, Goldberg VM, Rimnac CM, Doerschuk CM, et al. The balance between endotoxin accumulation and clearance during particle-induced osteolysis in murine calvaria. J Orthop Res 2007;25:361–9.
47. Taki N, Tatro JM, Lowe R, Goldberg VM, Greenfield EM. Comparison of the roles of IL-1, IL-6, and TNFα in cell culture and murine models of aseptic loosening. Bone 2007;40:1276–83.

ORTHOSuperSite

Evaluation of Biomechanical and Histological Features of Vertebrae Following Vertebroplasty Using Hydroxyapatite Blocks

By Masashi Oshima, MD; Hiromi Matsuzaki, MD; Yasuaki Tokuhashi, MD; Akihiro Okawa, MD

Abstract

Vertebroplasty was performed using hydroxyapatite blocks to examine the course of compressive strength and histological features in a dog model. The vertebral fracture model was prepared by punching a hole in the center of the vertebra and at 4 sites around the vertebra (5 holes in total) from the front side of the vertebra using an air drill and hollowing the holes. Measurements were made on healthy vertebrae, vertebrae from the vertebral fracture model, vertebrae removed from animals immediately after vertebroplasty, vertebrae collected 1 and 2 month after vertebroplasty, and vertebrae untreated for 1 month after vertebral fracture. Histological examinations were also performed 1 and 2 weeks and 1 and 2 months after vertebroplasty with hydroxyapatite blocks. The strength of vertebrae in the fracture model immediately after vertebroplasty was significantly higher than that in the untreated fracture, and the strength of vertebrae 1 month after the procedure was equivalent to that of healthy vertebrae. Histologically, new bone formation was found around hydroxyapatite blocks 2 weeks after the procedure, and strong crosslinking between neighboring hydroxyapatite blocks was found after 1 month.

These results suggest that hydroxyapatite blocks may be effective as filling material for vertebral fracture from both biomechanical and histological perspectives.

Vertebra repair at the pedicle of the vertebral arch using polymethylmethacrylate (PMMA),[1,2] calcium phosphate cement,[3] and hydroxyapatite blocks[4] is of interest as a minimally invasive treatment for fracture. Hydroxyapatite blocks are significantly superior to other materials in terms of dynamic strength, bone affinity, filling technique, and complications, since the vertebra can be repaired by filling with box-shaped hydroxyapatite blocks with no risk of the blocks flowing into blood vessels.[4] However, changes over time in the dynamic strength of vertebrae filled with hydroxyapatite blocks and histological changes after vertebroplasty have not been examined. Therefore, in this study, we prepared a dog model of lumber vertebral fracture and examined the dynamic strength and histological characteristics of vertebrae 1 and 2 weeks and 1 and 2 months after vertebroplasty using hydroxyapatite blocks.

Materials and Methods

Eight 6-month-old beagles were used in the study. Anesthesia was performed by gradual administration of 50 mg of double-diluted 5% pentobarbiturate into a vein. General anesthesia was ensured by adding the anesthetic agent as needed based on monitoring of the

depth of anesthesia. A transperitoneal approach was taken after a midsagittal incision in the abdominal region. After turning the aorta abdominalis to the side and tying up the segmental artery and vein, we approached the front side of the lumber vertebra. The vertebral fracture model was prepared by punching a hole in the center of the vertebra and at 4 sites around the vertebra (5 holes in total) from the front side of the vertebra using a 3-mm air drill and hollowing the holes. The study was performed after obtaining approval from our institutional ethical committee for preclinical studies.

Vertebral repair was performed using hydroxyapatite blocks developed for dogs (HOYA Co, Tokyo, Japan) with a porosity of 30% and a size of 2.0×2.0×3.6 mm with 1 sloping face. The inner cavity of the vertebra in the vertebral fracture model was filled firmly with hydroxyapatite blocks from a hole prepared in the front side of the vertebra using an impactor (Figure 1). Each vertebra was filled with 12 to 22 hydroxyapatite blocks (15.5±2.5). The percentage occupation of the hydroxyapatite blocks (total volume of hydroxyapatite blocks in the vertebra/volume of the vertebra) was 27% to 34% (30.7±2.6). Plain radiographs obtained after the procedure are shown in Figure 2. Neighboring vertebrae were used as controls.

Animals were sacrificed at 1 week, 2 weeks, 1 month, and 2 months after vertebroplasty, and vertebrae were removed for measurement of the dynamic strength. Measurements were made on 16 healthy vertebrae, 6 vertebrae removed prior to treatment of vertebral fracture, 14 removed from animals immediately after vertebroplasty, 4 collected 1 month after vertebroplasty, 4 collected 2 months after vertebroplasty, and 2 untreated for 1 month after vertebral fracture. An Autograph DSS-5000 system (Shimadzu Co, Kyoto, Japan) was used for measurement of the maximum compressive strength using a 5 t load cell, a full scale of 500 kgf, and a test speed of 5 mm/min (Figure 3).

A Mann-Whitney *U* test was used for statistical analysis with $P<.01$ considered a significant difference.

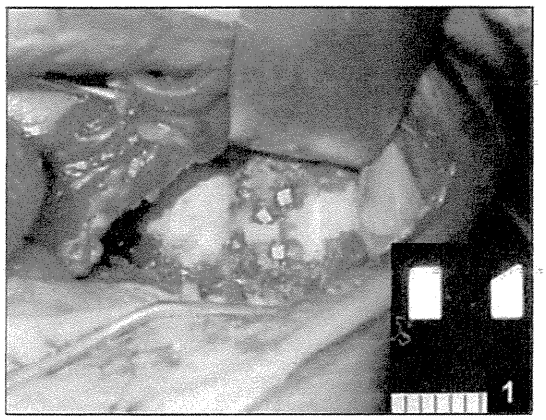

Figure 1: Hydroxyapatite block and surgical findings after vertebroplasty with hydroxyapatite blocks in the vertebral fracture model.

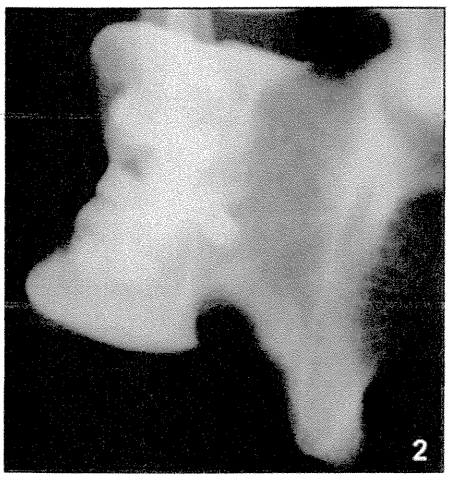

Figure 2: Plain radiographs after vertebroplasty with hydroxyapatite blocks.

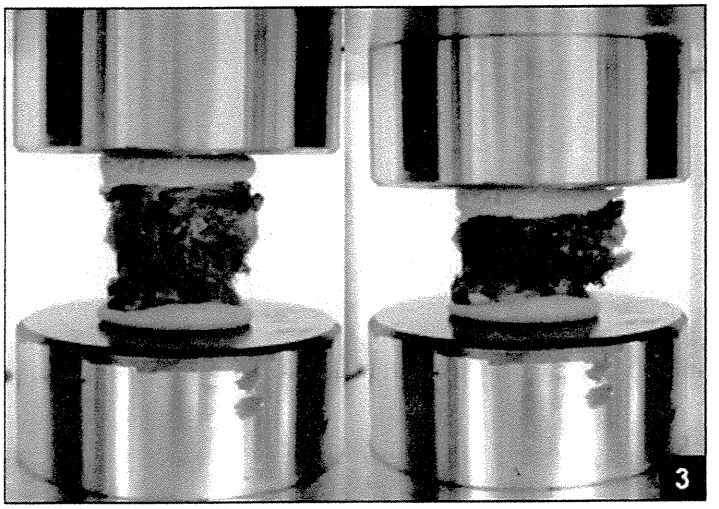

Figure 3: Measurement of maximum compressive strength.

A histological examination was performed on 2 vertebrae removed from the subjects at 1 week, 2 weeks, and 1 month after vertebroplasty. The vertebrae were cut by the sagittal cutting method to prepare test samples, and toluidine blue staining was performed.

Results

The average bone density of vertebrae measured using dual-energy x-ray absorptiometry was 0.54±0.02 g/cm^2 and did not differ significantly among the vertebrae. Measurement of the maximum compressive strength showed average strengths of 238.4±36.76 kgf for healthy vertebra, 118.3±12.51 kgf for untreated vertebrae in the model of vertebral fracture, 150.7±20.51 kgf for vertebrae immediately after vertebroplasty with hydroxyapatite blocks, 228.0±20.01 kgf at 1 month after vertebroplasty, 263.0±26.53 kgf at 2 months after vertebroplasty, and 278±21.21 kgf at 1 month untreated after vertebral fracture (Figure 4).

A significant difference was noted in compressive strength between fractured vertebrae and vertebrae immediately after vertebroplasty with hydroxyapatite blocks (P<.01). The vertebrae immediately after vertebroplasty were significantly weaker than healthy vertebra (P<.01), but no significant difference was noted in the strength of the repaired vertebrae and healthy vertebrae at 1 or 2 months after the procedure.

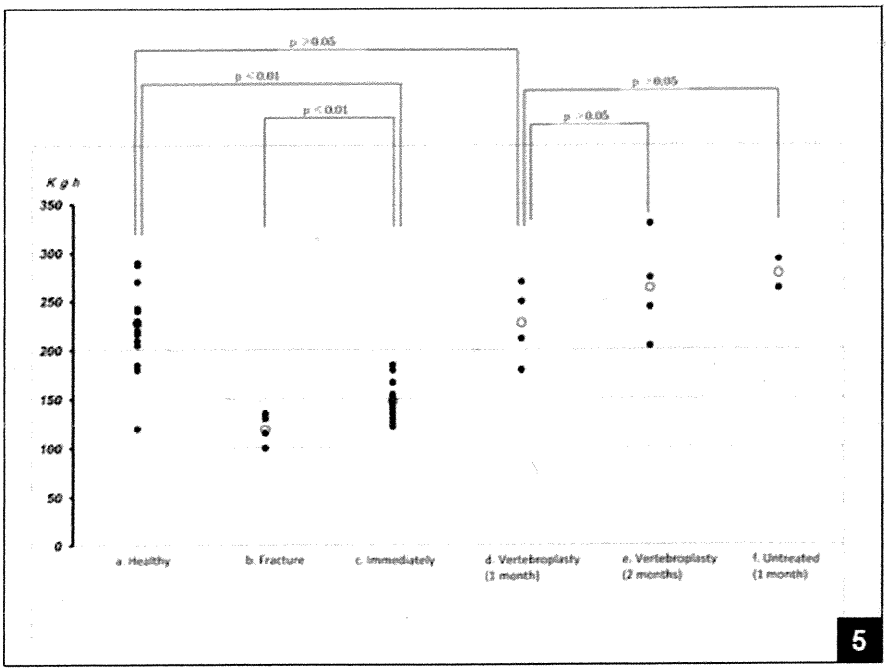

Figure 4: Measurement of compressive strength of healthy vertebrae (a), vertebrae from the vertebral fracture model (b), vertebrae immediately after filling with hydroxyapatite blocks (c), vertebrae 1 month after filling with hydroxyapatite blocks (d), vertebrae 2 months after filling with hydroxyapatite blocks (e), and untreated vertebrae after 1 month (f).

In vertebrae observed 1 week after filling with hydroxyapatite blocks, bone tissues that were assumed to have been broken during vertebroplasty were observed around the hydroxyapatite blocks. Two weeks after vertebroplasty, development of new bone was observed around parts of the hydroxyapatite blocks (Figure 5), and after 1 month the amount of new bone had increased with firm crosslinking between neighboring hydroxyapatite blocks (Figure 6).

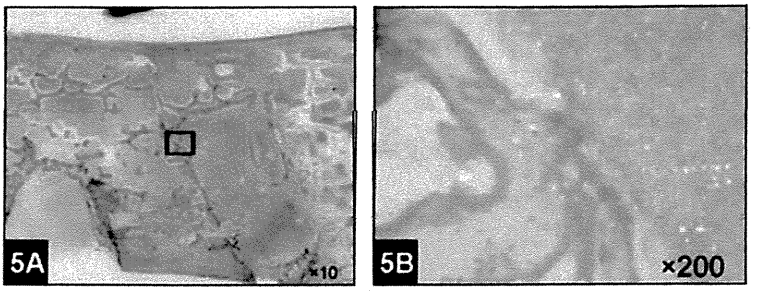

Figure 5: Development of new bone was found in the area around the hydroxyapatite blocks 2 weeks after vertebroplasty.

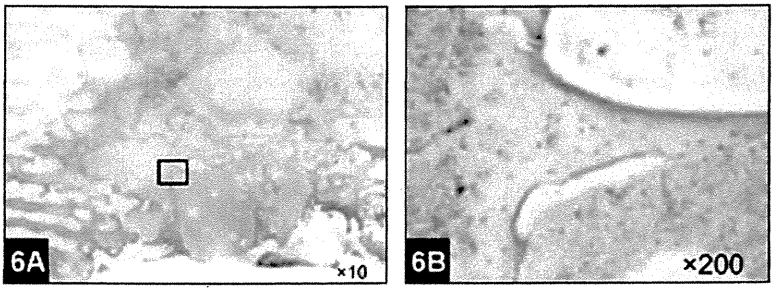

Figure 6: Crosslinking of new bone was found 1 month after vertebroplasty with hydroxyapatite blocks in the fracture model.

Discussion

Synostosis and pseudoarthrosis may develop in cases of compression fracture at a thoracolumbar lesion in which a heavy burden is placed on a vertebra. Local kyphotic deformation may also be facilitated, and the crushed vertebra may point into the vertebral canal and induce a nervous disorder.[5]

In fresh fractures of the spine, Taneichi et al[6] found symptoms of progressively crushed vertebrae after vertebral fracture and nervous disorders in 36% and 3% of cases, respectively. The biomechanical characteristics of a thoracolumbar lesion include an excessive anterior load as large as 70% and a small posterior load as little as 30%.[5,7] Based on these data, redevelopment of the anterior support system is necessary in treatment of a disease with anterior load failure at a thoracolumbar lesion. Thus, vertebral repair at the pedicle of the vertebral arch is a minimally invasive method that can be used clinically in the early postoperative period.

Polymethylmethacrylate, calcium phosphate cement, and hydroxyapatite blocks have been used as filling material in vertebroplasty. However, these materials have problems of surgical usage, safety, bone affinity, and cost.

In vertebroplasty performed using PMMA or calcium phosphate cement in a fracture model of cadaveric thoracolumbar vertebral bodies, Lim et al[8] found that failure against compressive loads increased significantly with PMMA compared to normal vertebrae, whereas compressive stiffness decreased significantly with calcium phosphate cement compared to PMMA and normal vertebrae.

Tomita et al[9] compared the strength and stiffness of individual vertebrae after vertebroplasty for thoracic and lumbar vertebrae in female cadavers using PMMA and calcium phosphate cement. The postoperative strength increased significantly with vertebroplasty for thoracic vertebrae using PMMA, and a significant decrease in postoperative stiffness was found after vertebroplasty for lumbar vertebrae using PMMA and for thoracic and lumbar vertebrae using calcium phosphate cement. Turner et al[10] compared compressive strength 1 and 6 months after vertebroplasty in dog vertebrae using calcium phosphate cement and PMMA. With calcium phosphate cement, the strength at 6 months postoperatively was greater than that at 1 month; whereas with PMMA, the strength at 6 months was less than at 1 month, although the difference was not significant.

The compressive strength and histology after vertebroplasty with hydroxyapatite blocks have not been examined prior to the present study. We found that the compressive strength of vertebrae in a model of vertebral fracture increased significantly after vertebroplasty performed using hydroxyapatite blocks. This may be because the compressive strength of fractured vertebrae increased after destroyed

bone trabeculae of cancellous bone were replaced by hydroxyapatite blocks. However, in the early phase after vertebroplasty, the dynamic strength was not equivalent to that of healthy bone, which may be related to breakage of the anterior wall of the vertebra, the strength of the hydroxyapatite blocks, and differences in the strength of histological bonds.

In vertebroplasty with hydroxyapatite blocks, the dynamic strength has been shown to depend on the form and porosity of the hydroxyapatite blocks. Matsuzaki[4] performed a compressive load test to determine the appropriate block size to maintain an orthodontic force and found that a block of 4 to 5.6 mm was superior. In addition, the effect on vertebral reposition was maximized with a block with 1 sloping face because such blocks can converge into a so-called "stone wall-like form." Hydroxyapatite is also more effective than PMMA due to facilitation of osseous conduction.

It is thought to be difficult for new bones to develop in the blocks when the porosity of the block is decreased to increase the strength, and thus the strength of the crosslinking bond may be decreased. In our study, a porosity of 30% was used to ensure sufficient strength to avoid breakage of hydroxyapatite blocks following filling of vertebrae.

In a biomechanical study, Belkoff et al[11] showed that the compressive strength of a fractured vertebra after filling with bone cement was higher than that of healthy bone. However, the risk of fracture in neighboring vertebrae may be increased by increasing the strength of the fractured vertebra[12]; and there is no consensus on the appropriate compressive strength of vertebrae in vertebroplasty.

In the vertebroplasty performed in the present study, a strength greater than that of the model bone fracture was achieved, but vertebrae filled with hydroxyapatite blocks were not as strong as healthy vertebrae in the early phase. However, a strength equivalent to that of healthy vertebrae was obtained 1 month after vertebroplasty. A further study is required to determine the ideal strength of vertebrae in the early phase and the changes in strength over time.

Histologically, development of new bone around hydroxyapatite blocks was found in the model of vertebral fracture 2 weeks after vertebroplasty, and crosslinking of new bone was confirmed between neighboring hydroxyapatite blocks after 1 month. These findings are consistent with the compressive strength of the vertebrae, which was higher after 1 month than immediately after vertebroplasty and became equivalent to that of healthy vertebrae.

Urrutia et al[13] reported osteonecrosis in approximately 50% of rabbits in which vertebroplasty was performed with PMMA, based on a histological examination performed in the early phase. In the present study, no osteonecrosis was found in the tissues of individual vertebrae for which vertebroplasty was performed using hydroxyapatite blocks. The strength of vertebrae in the early phase after vertebroplasty with PMMA has been shown to be higher than that after vertebroplasty using calcium phosphate cement, but the subsequent compressive strength is unclear.

Turner et al[10] suggested that the strength decreased with PMMA 6 months postoperatively, and histological factors such as osteonecrosis may be involved in this observation. However, it is apparent that hydroxyapatite permits osseous conduction and that strength is increased by development of new bone over time, compared with PMMA. In our study, strength was increased by crosslinking of new bone 2 months postoperatively, and further examination of long-term dynamic strength and histological changes, including an evaluation of porosity, may help to optimize the procedure of vertebroplasty with hydroxyapatite blocks.

Conclusion

Our study addressed the difference in regeneration potential between healthy and osteoporotic vertebrae. Generally, an osteoporosis model should be prepared using oophorectomy and calcium-free dieting, but this requires a long period of time, and such models also have large individual variability. In our study, young dogs were used with the aim of reducing individual variability of vertebral strength, and vertebroplasty was evaluated using hydroxyapatite blocks. Vertebral collapse and bone adhesion in patients with osteoporosis-related vertebral body fracture require evaluation over a long period, and the clinical course is completely different from that in a healthy vertebra model. However, vertebroplasty performed with hydroxyapatite blocks for improvement of bone strength in the early phase of bone fracture will be effective for improving the dynamic strength of vertebrae using anterior support, and thus is important for treatment of osteoporosis-related vertebral fracture. We plan to perform a similar study using an osteoporosis model.

References

1. Gangi A, Kastler BA, Dietemann JL. Percutaneous vertebroplasty guided by a combination of CT and fluoroscopy. *AJNR Am J Neuroradiol.* 1994; 15(1):83-86.
2. Jensen ME, Evans AJ, Mathis JM, Kallmes DF, Cloft HJ, Dion JE. Percutaneous polymethylmethacrylate vertebroplasty in the treatment of osteoporotic vertebral body compression fractures; technical aspects. *AJNR Am J Neuroradiol.* 1997; 18(10):1897-1904.
3. Yamamoto H, Shibata T, Ikeuchi M. Calcium phosphate cement for osteoporotic vertebral fracture [in Japanese]. *Rinsho Seikei Geka.* 1999; 34(4):435-442.
4. Matsuzaki H. New transpedicular kyphoplasty using hydroxyapatite for vertebral fracture [in Japanese]. *J Musculoskeletal System.* 2002; 15(3):247-253.

5. Ito M. Biomechanics of osteoporotic spinal compressive fracture [in Japanese]. *Spine and Spinal Cord*. 2003; 16(9):927-932.
6. Taneichi H, Kaneda K, Oguma T, Okaji M. Risk factor analysis for osteoporotic vertebral collapse and pseudoarthrosis [in Japanese]. *Rinsho Seikei Geka*. 2002; 37:437-442.
7. Haher TR, Tozzi JM, Lospinuso MF, et al. The contribution of the three columns of the spine to spinal stability: a biomechanical model. *Paraplegia*. 1989; 27(6):432-439.
8. Lim TH, Brebach GT, Renner SM, et al. Biomechanical evaluation of an injectable calcium phosphate cement for vertebroplasty. *Spine (Phila Pa 1976)*. 2002; 27(12):1297-1302.
9. Tomita S, Molloy S, Jasper LE, Abe M, Belkoff SM. Biomechanical comparison of kyphoplasty with different bone cements. *Spine (Phila Pa 1976)*. 2004; 29(11):1203-1207.
10. Turner TM, Urban RM, Singh K, et al. Vertebroplasty comparing injectable calcium phosphate cement compared with polymethylmethacrylate in a unique canine vertebral body large defect model. *Spine J*. 2008; 8(3):482-487.
11. Belkoff SM, Mathis JM, Jasper LE, Deramond H. The biomechanics of vertebroplasty. The effect of cement volume on mechanical behavior. *Spine (Phila Pa 1976)*. 2001; 26(14):1537-1541.
12. Grados F, Depriester C, Cayrolle G, Hardy N, Deramond H, Fardellone P. Long-term observations vertebral osteoporotic fractures treated by percutaneous vertebroplasty. Rheumatology (Oxford). 2000; 39(12):1410-1414.
13. Urrutia J, Bono CM, Mery P, Rojas C. Early histologic changes following polymethylmethacrylate injection (vertebroplasty) in rabbit lumbar vertebrae. *Spine (Phila Pa 1976)*. 2008; 33(8):877-882.

Authors

Drs Oshima, Matsuzaki, Tokuhashi, and Okawa are from the Department of Orthopedic Surgery, Nihon University, Tokyo, Japan.

Drs Oshima, Matsuzaki, Tokuhashi, and Okawa have no relevant financial relationships to disclose.

Correspondence should be addressed to: Masashi Oshima, MD, Department of Orthopedic Surgery, Nihon University, 30-1, Oyaguchi, Kami-cho, Itabashi-ku, Tokyo, Japan.

doi: 10.3928/01477447-20100104-15

Published April 5, 2010

JEM

Article

The Blimp1–Bcl6 axis is critical to regulate osteoclast differentiation and bone homeostasis

Yoshiteru Miyauchi,[1] Ken Ninomiya,[1] Hiroya Miyamoto,[1] Akemi Sakamoto,[6] Ryotaro Iwasaki,[3] Hiroko Hoshi,[1] Kana Miyamoto,[1] Wu Hao,[1] Shigeyuki Yoshida,[3] Hideo Morioka,[1] Kazuhiro Chiba,[1] Shigeaki Kato,[7] Takeshi Tokuhisa,[6] Mitinori Saitou,[8] Yoshiaki Toyama,[1] Toshio Suda,[4] and Takeshi Miyamoto[1,2,5,9]

[1]Department of Orthopedic Surgery, [2]Department of Integrated Bone Metabolism and Immunology, [3]Department of Dentistry and Oral Surgery, [4]Department of Cell Differentiation, The Sakaguchi Laboratory of Developmental Biology, [5]Keio Kanrinmaru Project, Keio University School of Medicine, Shinjuku-ku, Tokyo 160-8582, Japan
[6]Department of Developmental Genetics, Graduate School of Medicine, Chiba University, Chiba 260-8670, Japan
[7]Institute of Molecular and Cellular Bioscience, University of Tokyo, Bunkyo-ku, Tokyo 113-0032, Japan
[8]Department of Anatomy and Cell Biology, Graduate School of Medicine, Kyoto University, Yoshida-Konoe-cho, Sakyo-ku, Kyoto 606-8501, Japan
[9]Precursory Research for Embryonic Science and Technology, Japan Science and Technology Agency, Kawaguchi, Saitama 332-0012, Japan

Controlling osteoclastogenesis is critical to maintain physiological bone homeostasis and prevent skeletal disorders. Although signaling activating nuclear factor of activated T cells 1 (NFATc1), a transcription factor essential for osteoclastogenesis, has been intensively investigated, factors antagonistic to NFATc1 in osteoclasts have not been characterized. Here, we describe a novel pathway that maintains bone homeostasis via two transcriptional repressors, B cell lymphoma 6 (Bcl6) and B lymphocyte–induced maturation protein-1 (Blimp1). We show that Bcl6 directly targets 'osteoclastic' molecules such as NFATc1, cathepsin K, and dendritic cell-specific transmembrane protein (DC-STAMP), all of which are targets of NFATc1. Bcl6-overexpression inhibited osteoclastogenesis in vitro, whereas Bcl6-deficient mice showed accelerated osteoclast differentiation and severe osteoporosis. We report that Bcl6 is a direct target of Blimp1 and that mice lacking Blimp1 in osteoclasts exhibit osteopetrosis caused by impaired osteoclastogenesis resulting from Bcl6 up-regulation. Indeed, mice doubly mutant in Blimp1 and Bcl6 in osteoclasts exhibited decreased bone mass with increased osteoclastogenesis relative to osteoclast-specific Blimp1-deficient mice. These results reveal a Blimp1–Bcl6–osteoclastic molecule axis, which critically regulates bone homeostasis by controlling osteoclastogenesis and may provide a molecular basis for novel therapeutic strategies.

CORRESPONDENCE
Takeshi Miyamoto:
miyamoto@sc.itc.keio.ac.jp

Abbreviations used: Bcl6, B cell lymphoma 6; Blimp1, B lymphocyte–induced maturation protein 1; BMM, BM macrophage; ChIP, chromatin immunoprecipitation; cKO, conditional KO; Ctsk, cathepsin K; DC-STAMP, DC-specific transmembrane protein; DKO, double KO; NFATc1, nuclear factor of activated T cells 1; PGC, primordial germ cell; RANKL, receptor activator of NF-κB ligand; TRAP, tartrate-resistant acid phosphatase.

Osteoclasts are responsible for bone resorption, and thereby play an essential role in maintaining bone volume and homeostasis (Karsenty and Wagner, 2002). Dysregulation of osteoclast differentiation or function disrupts maintenance of bone homeostasis, which in turn leads to pathogenic conditions such as osteoporosis, rheumatoid arthritis, lytic bone metastases, or Paget's bone disease (Rodan and Martin, 2000). Thus, osteoclasts could potentially be targeted therapeutically to treat skeletal disorders. Osteoclasts originate from BM–derived monocyte/macrophage precursor cells of hematopoietic origin and are differentiated by signaling through the receptor activator of NF-κB ligand (RANKL; Kong et al., 1999). RANKL induces osteoclast differentiation by activating the nuclear factor of activated T cells 1 (NFATc1),

Y. Miyauchi and K. Ninomiya contributed equally to this paper.

The Rockefeller University Press $30.00
J. Exp. Med. Vol. 207 No. 4 751-762
www.jem.org/cgi/doi/10.1084/jem.20091957

Published April 5, 2010

JEM

a transcription factor required for osteoclastogenesis (Takayanagi et al., 2002; Koga et al., 2004; Sato et al., 2006; Shinohara et al., 2008). Activated NFATc1 induces expression of "osteoclastic" molecules essential for osteoclast differentiation and function, such as DC-specific transmembrane protein (DC-STAMP) to facilitate cell–cell fusion, cathepsin K (Ctsk) to promote bone matrix proteolysis, and NFATc1 to drive differentiation (Yagi et al., 2005; Li et al., 2006). Thus, signaling pathways mediated by positive regulators of NFATc1 in osteoclastogenesis have been intensively studied, whereas factors negatively modulating osteoclastogenesis are largely unknown.

B lymphocyte–induced maturation protein 1 (Blimp1) has been investigated in numerous cell types (John and Garrett-Sinha, 2009) and is reportedly essential for specification and maintenance of primordial germ cells (PGCs) through silencing of somatic programs (Ohinata et al., 2005). B cell lymphoma 6 (Bcl6) was originally identified as a protooncogene because its chromosomal translocation and constitutive expression promotes lymphomagenesis (Ohno, 2006). *Bcl6*$^{-/-}$ mice show impaired germinal center formation (Fukuda et al., 1997). The roles of Blimp1 and Bcl6 have also been investigated in B cell and plasma cell development (Turner et al., 1994; Fukuda et al., 1997), as well as in T cells (Dent et al., 1998; Kusam et al., 2003; Ichii et al., 2004; Kallies et al., 2006; Martins et al., 2006; Cimmino et al., 2008). However, the roles of Blimp1 and Bcl6, both of which are transcriptional repressors, have not previously been characterized in osteoclastogenesis or skeletal disorders, although mutations in Bcl6-associated molecules are reportedly seen in skeletal pathologies such as malformation of fingers and clavicles (Ng et al., 2004). Recently, it was reported that inhibiting NFATc1 using the NFATc1 inhibitor FK506 actually resulted in reduced bone mass caused by inhibition of bone formation that was more potent than inhibition of osteoclastogenesis (Koga et al., 2005). Therefore, additional regulators of osteoclast differentiation have been sought as factors that could potentially increase bone mass.

In this study, we identify two transcriptional repressors controlling osteoclastogenesis, Bcl6 and Blimp1. We show that Bcl6 negatively regulates expression of osteoclastic genes, i.e., *NFATc1*, *DC-STAMP*, and *Ctsk*, which are all NFATc1 targets. We found that Bcl6 is recruited to promoters of these genes, and that Bcl6 inhibits osteoclastogenesis. We also report that Blimp1 binds to the *Bcl6* promoter, likely suppressing its expression. Bcl6-deficient mice exhibited decreased bone mass with increased osteoclastogenesis, whereas osteoclast-specific Blimp1 conditional KO (cKO) mice showed impaired osteoclast differentiation and increased bone mass, likely resulting from Bcl6 dysregulation. Overall, our data demonstrate that an axis of transcriptional repressors is crucial to regulate osteoclastogenesis and bone homeostasis.

RESULTS

Bcl6 is a negative regulator of osteoclastogenesis

RANKL stimulates osteoclastogenesis by activating NFATc1 (Takayanagi et al., 2002; Koga et al., 2004; Sato et al., 2006; Shinohara et al., 2008). To identify genes potentially suppressed after RANKL stimulation of osteoclast precursor cells (BM macrophages [BMMs]), we undertook comparative microarray screens of BMMs treated with or without RANKL and found that expression of the transcriptional repressor *Bcl6* was down-regulated by RANKL (Fig. 1 A). *Bcl6* down-regulation by RANKL was confirmed by real-time RT-PCR, immunofluorescence, and immunoblot analysis (Fig. S1 and Fig. 1 B). Immunofluorescence analysis showed that Bcl6 was detected in the nuclei of M-CSF–dependent macrophages, but not in nuclei of multinuclear osteoclasts induced by RANKL (Fig. 1 B). Interestingly, chromatin immunoprecipitation (ChIP) assays showed that, in the absence of RANKL, Bcl6 was recruited to the *NFATc1* P1 promoter, a region critical for regulating *NFATc1* expression in osteoclasts, and was dismissed from the promoter after RANKL treatment. In contrast, NFATc1, an essential positive regulator of osteoclastogenesis, was absent from the *NFATc1* P1 promoter in the absence of RANKL, but recruited after RANKL stimulation (Fig. 1 C). These results suggest a potential role of Bcl6 in inhibiting osteoclastogenesis. Bcl6 overexpression also potently inhibited osteoclast differentiation in vitro (Fig. 1 D), suggesting that Bcl6 negatively regulates osteoclast differentiation and that its down-regulation after RANKL stimulation is critical to induce osteoclastogenesis.

Bcl6 deficiency facilitates osteoclast formation

To characterize the physiological roles of Bcl6 in osteoclastogenesis, we analyzed Bcl6-deficient (*Bcl6*$^{-/-}$) mice. *Bcl6*$^{-/-}$ mice exhibited lower bone mass as detected by microradiographical and dual-energy x-ray absorptiometry analysis compared with heterozygous littermates (*Bcl6*$^{+/-}$; Fig. 2, A and B). Consistently, histomorphometric analysis of *Bcl6*$^{-/-}$ mice demonstrated increased osteoclastogenesis and large osteoclast formation in *Bcl6*$^{-/-}$ mice. *Bcl6*$^{-/-}$ mice also showed elevated levels of serum C-terminal telopeptides of type I collagen (CTx) and decreased bone parameters (Fig. 2, C and D, and Fig. S2). In vitro, osteoclast progenitor cells isolated from Bcl6-deficient mice and treated with RANKL differentiated more rapidly into multinuclear tartrate-resistant acid phosphatase (TRAP)–positive cells than did those from control mice (Fig. 2 E and not depicted). Lower concentrations of RANKL not sufficient to differentiate control cells induced osteoclast differentiation of Bcl6-deficient cells (Fig. 2 E). Furthermore, increased bone resorbing activity was evident in Bcl6-deficient osteoclasts (Fig. 2 F), suggesting loss of a negative regulator of osteoclast function and differentiation. Deletion of Bcl6 in osteoclast precursor cells did not alter cell proliferation or induce apoptosis (Fig. S3). Thus, Bcl6 functions to regulate osteoclast differentiation and bone homeostasis, and its down-regulation by RANKL is required for osteoclast formation.

Blimp1 regulates Bcl6 expression and osteoclastogenesis

Next, we searched for a factor that might suppress Bcl6 during osteoclastogenesis and found that the transcriptional

Published April 5, 2010

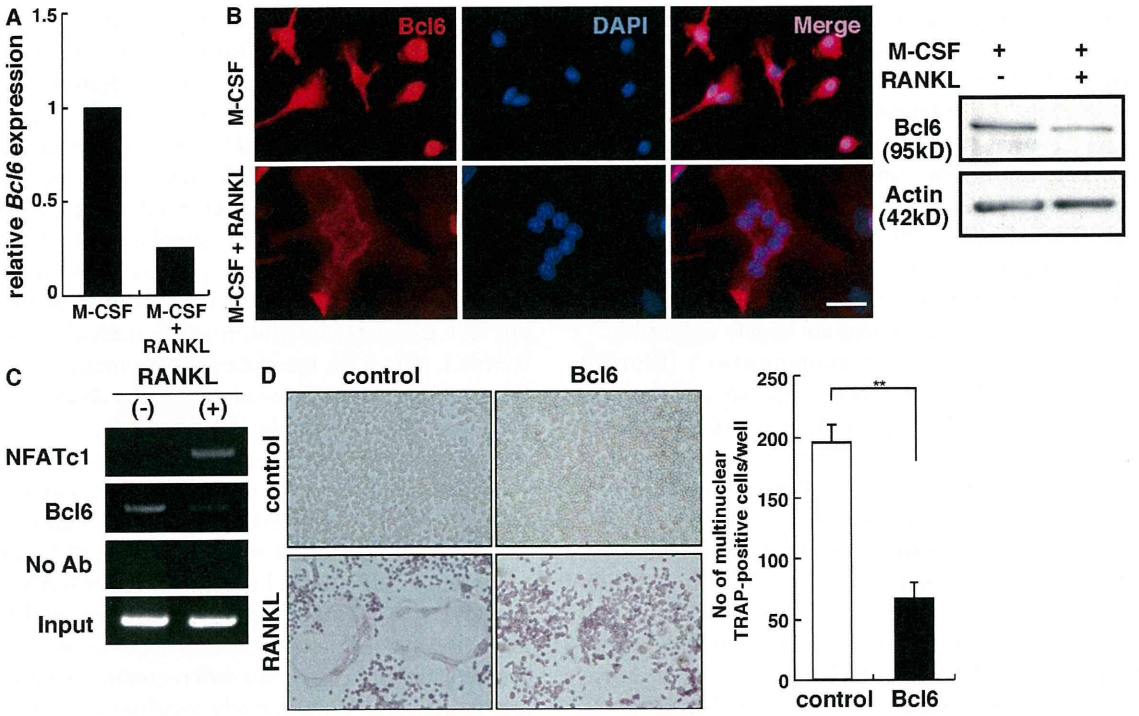

Figure 1. Bcl6 is suppressed during osteoclastogenesis and inhibits osteoclast formation. (A) *Bcl6* expression was examined by comparative microarray analysis between osteoclast precursors (M-CSF) and osteoclasts (M-CSF + RANKL) cultured for 6 d. (B) BMMs were cultured with or without RANKL for 8 d and subjected to immunofluorescence staining (left) and immunoblot (right) for Bcl6. Nuclei were visualized by DAPI. Bar, 25 µm. (C) Recruitment of NFATc1 and Bcl6 to the *NFATc1* P1 distal promoter was detected by ChIP assay. RAW264.7 cells were stimulated with or without RANKL for 48 h and subjected to ChIP analysis. (D) RAW264.7 cells transduced with Bcl6-overexpressing (Bcl6) or mock (control) retrovirus were cultured in the presence (RANKL) or absence (control) of RANKL for 5 d and stained with TRAP. Left, TRAP staining. (right) Numbers are means ± SD of multinuclear TRAP-positive cells in control or Bcl6-overexpressing RAW264.7 cells cultured with RANKL (**, $P < 0.001$; $n = 6$). Representative data of three independent experiments are shown (B–D).

repressor *Blimp1*, also called *Prdm1*, was specifically upregulated during osteoclast formation (Fig. S4 A). Blimp1 expression in osteoclasts was also demonstrated by using Blimp1-EGFP BAC transgenic mice, in which the EGFP sequence is knocked into the *Blimp1* locus, and by the observation that TRAP-positive cells showed Blimp1 expression (Fig. S4 B). RT-PCR analysis confirmed *Blimp1* induction in BMMs in the presence of RANKL in parallel with induction of *Ctsk*, a marker of osteoclast differentiation (Fig. 3 A). To determine whether Bcl6 is a Blimp1 target, an electrophoretic mobility shift assay (EMSA) was undertaken using a Bcl6 probe corresponding to a *Bcl6* regulatory region (Cimmino et al., 2008). Blimp1 formed a complex with the probe, but not with a Bcl6mut probe in which two nucleotides are changed to disrupt the Blimp1 binding sequence (Fig. S5 A). The PRDI probe, which corresponds to a region of the *interferon β* promoter known to bind Blimp1 protein (Keller and Maniatis, 1991) weakly but competitively, inhibited complex formation of the Bcl6 probe with Blimp1 (Fig. S5 A). In addition, unlabeled Bcl6 probe competed with labeled Bcl6 probe–Blimp1 to block complex formation, whereas unlabeled Bcl6mut probe did not (Fig. S5 A), confirming specificity and suggesting that Bcl6 is a direct Blimp1 target. Furthermore, ChIP analysis showed that, in the absence of RANKL, Blimp1 was absent from the *Bcl6* promoter, but was recruited there by RANKL treatment (Fig. S5 B). Thus, we conclude that Bcl6 is a direct target of Blimp1 in osteoclasts.

To investigate physiological roles of Blimp1 in osteoclast differentiation, we established osteoclast-specific Blimp1 cKO mice ($Ctsk^{Cre/+}Blimp1^{flox/-}$), as Blimp1-null mice are embryonic lethal (Vincent et al., 2005). Blimp1 heterozygotes ($Blimp1^{+/-}$) were crossed with Ctsk-Cre mice ($Ctsk^{Cre/+}$) in which *Cre* is knocked into the *Ctsk* locus (Nakamura et al., 2007). Next, $Ctsk^{Cre/+}Blimp1^{+/-}$ mice were crossed with a transgenic strain harboring *loxP*-flanked (floxed) *Blimp1* alleles ($Blimp1^{flox/flox}$; Ohinata et al., 2005) to yield Blimp1 cKO mice. $Ctsk^{Cre/+}Blimp1^{flox/+}$ mice served as controls. Blimp1 cKO mice showed increased trabecular bone mass and an expanded growth plate compared with control mice, as seen by histomorphometric and microradiographical analysis (Fig. 3, B–D). TRAP staining of bone sections and analysis of serum CTx levels demonstrated severe inhibition of TRAP-positive osteoclast formation and bone resorbing activity, respectively (Fig. 3, E and F). Bone-morphometric analysis revealed reduced osteoblastic parameters in Blimp1 cKO mice (Fig. 3 C). Differentiation of osteoblasts isolated from osteoclast-specific Blimp1 cKO mice did not differ

Published April 5, 2010

JEM

from that seen in control mice (Fig. S6), suggesting that Blimp1 deficiency in osteoclast progenitor cells promotes decreased osteoblast differentiation and bone formation. Deletion of Blimp1 in osteoclasts did not alter precursor cell proliferation or induction of apoptosis (Fig. S7, A and B). Furthermore, immune cell populations such as CD3-, B220-,

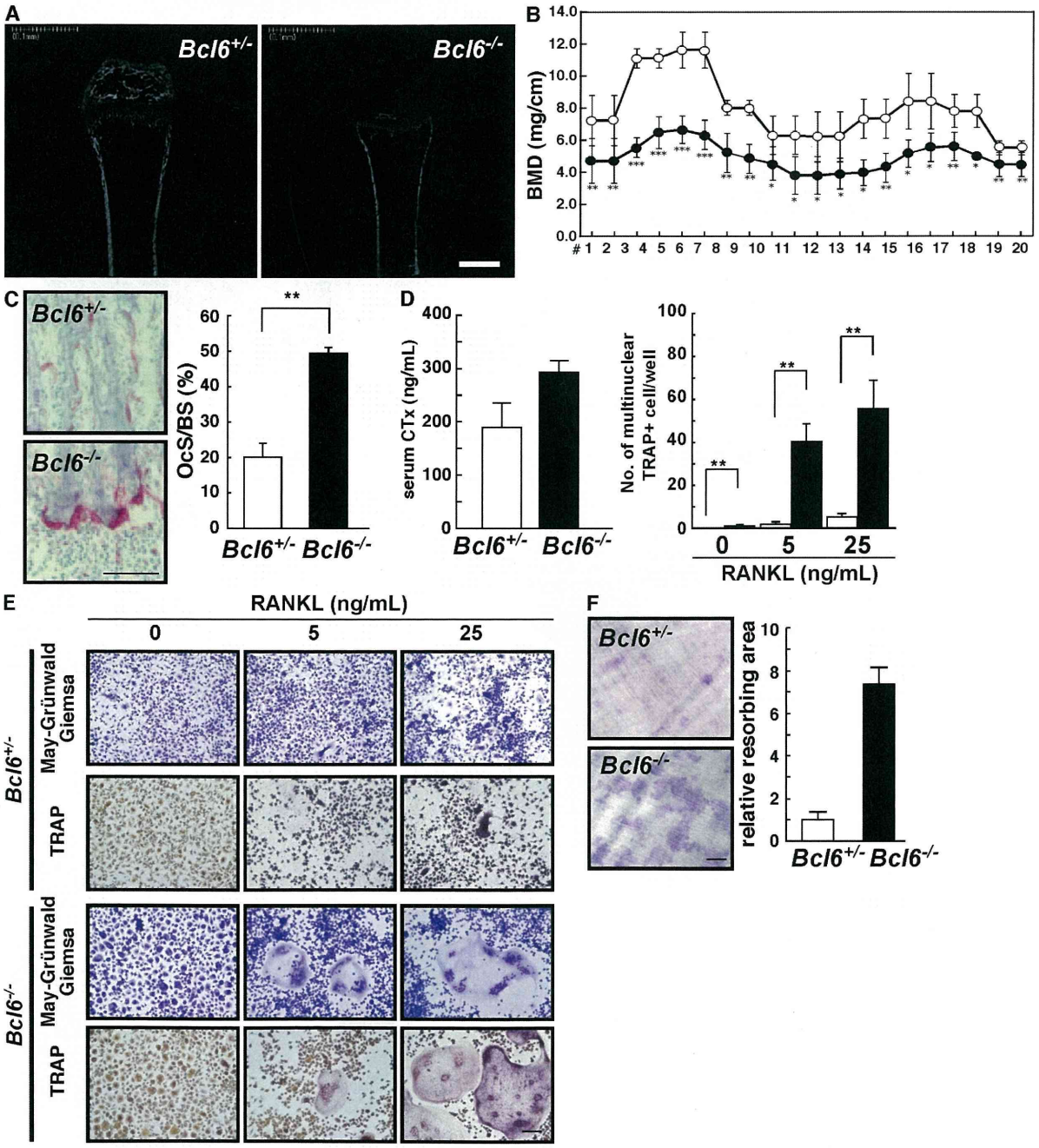

Figure 2. Increased osteoclast formation resulting from Bcl6 deficiency. (A) Micro focus CT analysis of femurs of *Bcl6*$^{+/-}$ (left) and *Bcl6*$^{-/-}$ (right) mice. (B) Bone mineral density (BMD) of equal longitudinal division of femurs of *Bcl6*$^{+/-}$ (open circles) and *Bcl6*$^{-/-}$ (closed circles) mice. Data are mean BMD (mg/cm^2) ± SD (*, $P < 0.05$; **, $P < 0.01$; ***, $P < 0.001$; $n = 3$). (C) TRAP staining of tibial sections of *Bcl6*$^{+/-}$ (top) and *Bcl6*$^{-/-}$ (bottom) mice, and osteoclast surface as a percentage of bone surface (OcS/BS). Data are means ± SD (**, $P < 0.001$; $n = 5$). (D) Serum levels of C-terminal teropeptides of type I collagen (CTx) were analyzed in *Bcl6*$^{+/-}$ (white bar) and *Bcl6*$^{-/-}$ (shaded bar) mice. Data are means ± SD (**, $P < 0.001$; $n = 3$). (E) Osteoclast precursor cells from control (*Bcl6*$^{+/-}$) or *Bcl6*$^{-/-}$ mice were cultured in the presence or absence of RANKL for 5 d and subjected to May-Grünwald Giemsa and TRAP staining, and the number of multinuclear TRAP-positive cells containing more than three nuclei was determined. Data are means ± SD of cells containing more than three nuclei (**, $P < 0.001$; $n = 3$). (F) Bone resorbing activity in *Bcl6*$^{+/-}$ (top) and *Bcl6*$^{-/-}$ (bottom) osteoclasts was analyzed by a pit formation assay. Representatives of at least three (E) and two (F) independent experiments are shown. Bars: (A) 1 mm; (C, E, and F) 100 µm.

Published April 5, 2010

Mac1-, or Gr1-positive cells were normal in the Blimp1 osteoclast-specific KO, suggesting that Blimp1 is required to regulate osteoclast differentiation and bone homeostasis (Fig. S8).

Severe inhibition of osteoclastogenesis was also observed in in vitro culture. Multinuclear TRAP-positive osteoclast formation induced by RANKL was significantly inhibited in Blimp1 cKO cells (Fig. 4, A and B). *Blimp1* expression was significantly up-regulated in the presence of RANKL in control cells; however, *Blimp1* induction was significantly inhibited in Blimp1 cKO cells (Fig. 4 C). In contrast, *Bcl6* expression was significantly down-regulated in control cells in the presence of RANKL; however, *Bcl6* expression in Blimp1 cKO cells was significantly up-regulated in Blimp1 cKO cells, even in the presence of RANKL (Fig. 4, C and D),

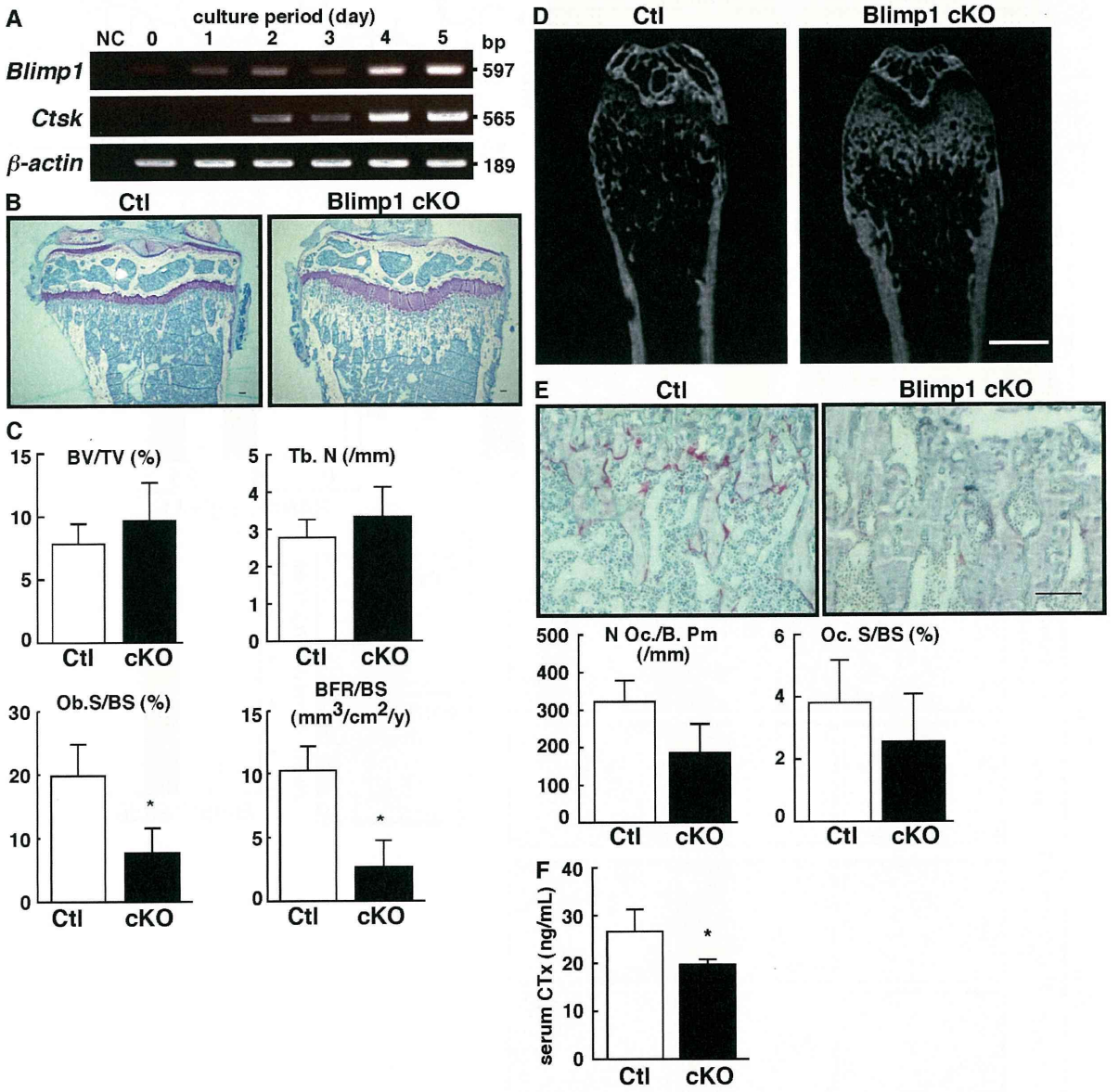

Figure 3. Blimp1 is essential for osteoclastogenesis and regulates bone homeostasis. (A) Total RNA isolated from BMMs cultured with M-CSF and RANKL for indicated periods was subjected to RT-PCR analysis with primers specific for *Blimp1* (top), *Ctsk* (middle), and *β-actin* (bottom). Representatives of at least three independent experiments are shown. (B–F) Bone phenotypes of osteoclast-specific Blimp1 KO (Blimp1 cKO) female mice at 8 wk old. (B) Longitudinal sections of tibias of control mice (Ctl; left) and Blimp1 cKO mice (right) were stained by toluidine blue. (C) Bone parameters are shown. Data are mean bone volume per total volume (BV/TV; %), trabecular number (Tb. N; /mm), osteoblast surface per bone surface (Ob.S/BS; %), or bone formation rate per bone surface (BFR/BS; $mm^3/cm^2/y$) ± SD of control (Ctl; white bar) and Blimp1 cKO (cKO; shaded bar) mice (*, $P < 0.01$; $n = 5$). (D) Microfocus CT analysis of femurs of control mice (Ctl; left) and Blimp1 cKO mice (right). (E) TRAP staining of tibial sections of control mice (Ctl; left) and Blimp1 cKO mice (right). Osteoclast parameters are shown as mean osteoclast number per bone perimeter (N.Oc/B.Pm) or osteoclast surface per bone surface (Oc.S/BS.) ± SD of control (Ctl; white bar) and Blimp1 cKO (cKO; shaded bar) mice ($n = 5$). (F) Serum CTx levels as a marker of bone resorption of control (Ctl; white bar) and Blimp1 cKO (cKO; shaded bar) mice (*, $P < 0.01$; $n = 5$). Bars: (B and E) 100 µm; (D) 1 mm.

Published April 5, 2010

suggesting that Blimp1 is critical to suppress *Bcl6* expression in osteoclasts during differentiation by RANKL and is essential for regulating osteoclastogenesis.

Bcl6 suppresses NFATc1 target genes during osteoclastogenesis

Expression of genes encoding osteoclastic factors, such as *NFATc1*, *DC-STAMP*, and *Ctsk*, all of which are targets of NFATc1 (Matsumoto et al., 2004; Asagiri et al., 2005; Yagi et al., 2007), was markedly inhibited in Blimp1 cKO osteoclasts (Fig. 5 A). It was shown by ChIP analysis that NFATc1 was not evident on osteoclastic gene promoters without RANKL, but was recruited there after RANKL treatment of control cells (Fig. 5 B). In contrast, in the absence of RANKL, Bcl6 was present on osteoclastic gene promoters, but was lost from those promoters after RANKL treatment of control

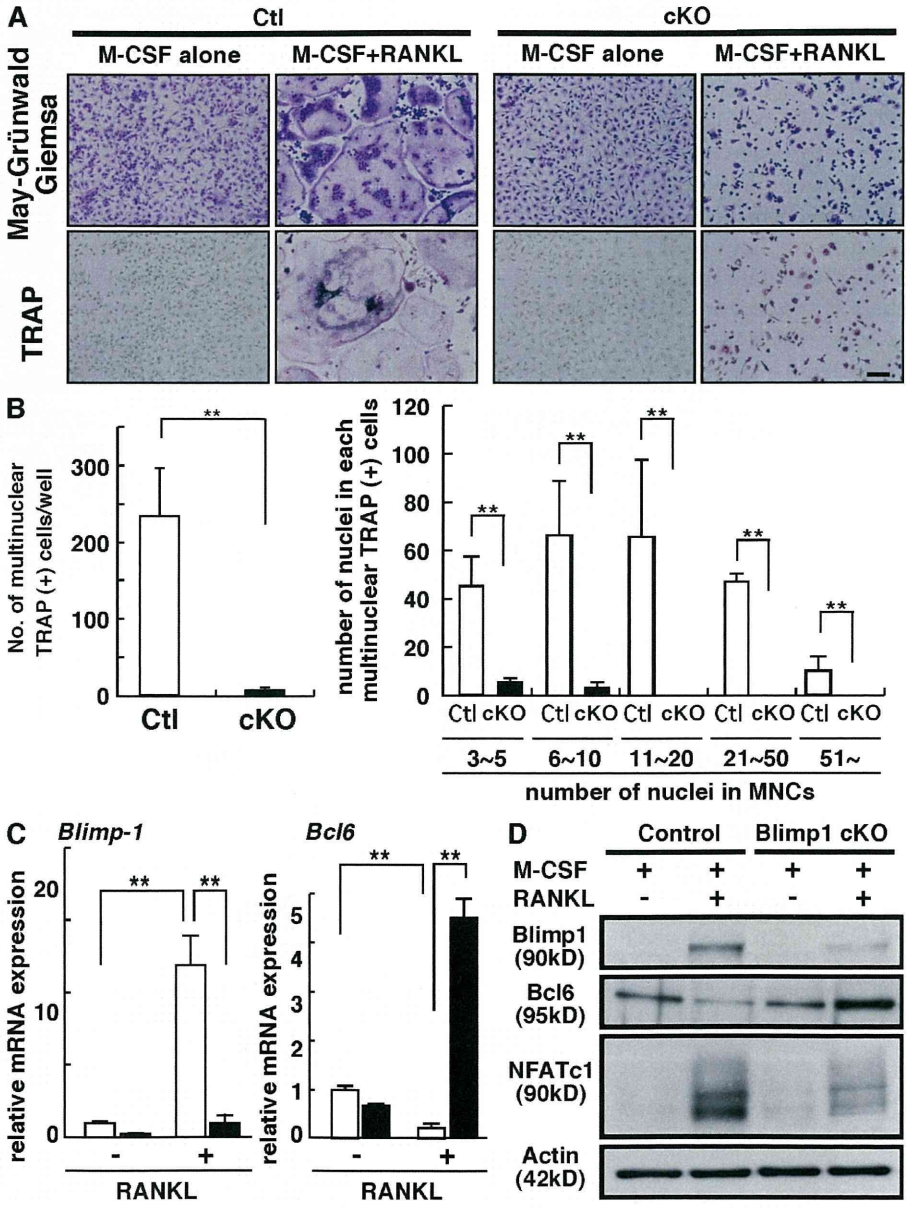

Figure 4. Impaired osteoclastogenesis and Bcl6 expression resulting from Blimp1 deficiency. (A–C) BMMs from control (Ctl) or Blimp1 cKO (cKO) mice were cultured in the presence or absence of RANKL for 8 d. Cells were then subjected to May-Grünwald Giemsa and TRAP staining (A), the number of TRAP-positive cells containing more than three nuclei was scored (B, left), and the number of nuclei in each multinuclear osteoclast was determined (B, right). Bar, 100 µm. Numbers are means ± SD of multinuclear cells (**, $P < 0.001$; $n = 3$). (C) Total RNA was prepared from control (white bars) or Blimp1 cKO (shaded bars) cells treated with (+) or without (−) RANKL, and *Blimp1* (left) or *Bcl6* (right) expression relative to *β-actin* was analyzed by quantitative real-time PCR. Data represent means ± SD of *Blimp1*/*β-actin* or *Bcl6*/*β-actin* levels (**, $P < 0.001$; $n = 4$). (D) Whole-cell lysates from control or Blimp1 cKO cells cultured with M-CSF alone or M-CSF plus RANKL were analyzed by immunoblotting to detect Blimp1, Bcl6, and NFATc1. Actin was analyzed as an internal control. Representatives of at least four independent experiments are shown.

Published April 5, 2010

cells (Fig. 5 B). These data strongly indicate that NFATc1 and Bcl6 are reciprocally recruited to osteoclastic gene promoters. Significantly, reciprocal recruitment of NFATc1 and Bcl6 was severely impaired in Blimp1 cKO cells (Fig. 5 B), suggesting that Blimp1 up-regulation is critical for loss of Bcl6 from osteoclastic promoters after RANKL stimulation. Bcl6 was not present on the *NFATc2* promoter, which is not activated by RANKL stimulation (Asagiri et al., 2005), in the presence or absence of RANKL (Fig. 5 B), suggesting that Bcl6 is selectively recruited to promoters of osteoclastic genes and inhibits osteoclast differentiation. Whereas Bcl6 was down-regulated by RANKL treatment in control cells, Bcl6 expression was maintained in Blimp1 cKO cells, even in the presence of RANKL (Fig. 4 C and Fig. S9). These data indicate that impaired Bcl6 down-regulation caused by loss of Blimp1 results in continuous inhibition of osteoclastic gene expression, which in turn promotes severe inhibition of osteoclastogenesis and increased bone mass.

Finally, to confirm the role of Blimp1 in regulating osteoclastogenesis through Bcl6, osteoclast-specific Blimp1/Bcl6 double KO mice (double KO [DKO]; $Ctsk^{Cre/+}Blimp1^{flox/-}Bcl6^{-/-}$ mice) were established (Fig. 6). DKO mice exhibited decreased bone mass in vivo compared with Blimp1 cKO mice (Fig. 6 A). Similarly, progenitor cells isolated from DKO mice showed accelerated osteoclastogenesis compared with those from Blimp1 cKO mice (Fig. 6, B and C), suggesting that Blimp1 regulates osteoclastogenesis in part through controlling Bcl6. These results reveal that the Blimp1–Bcl6–osteoclastic molecule axis is critical for controlling osteoclast differentiation and bone homeostasis (Fig. 7).

DISCUSSION

Here, we show that two transcriptional repressors, Bcl6 and Blimp1, are essential to control physiological osteoclast development and maintenance of bone homeostasis. Bcl6, a member of the POZ/BTB-zinc finger protein family, suppresses expression of "osteoclastic" genes, all of which are targets of NFATc1 (Matsumoto et al., 2004; Asagiri et al., 2005; Yagi et al., 2007), thereby antagonizing NFATc1 function. Indeed, NFATc1 deficiency in osteoclasts results in impaired differentiation (Asagiri et al., 2005), whereas Bcl6-deficient mice exhibit accelerated osteoclast formation and decreased bone mass. Blimp1, encoded by *Prdm1*, acts as a suppressor of Bcl6, likely by direct binding to the *Bcl6* promoter. In contrast to Bcl6-deficient mice, osteoclast-specific Blimp1 cKO mice display impaired osteoclast differentiation and increased bone mass. Expression of *Bcl6* and *Blimp1* is reciprocal in normal osteoclast formation, and unusual elevation

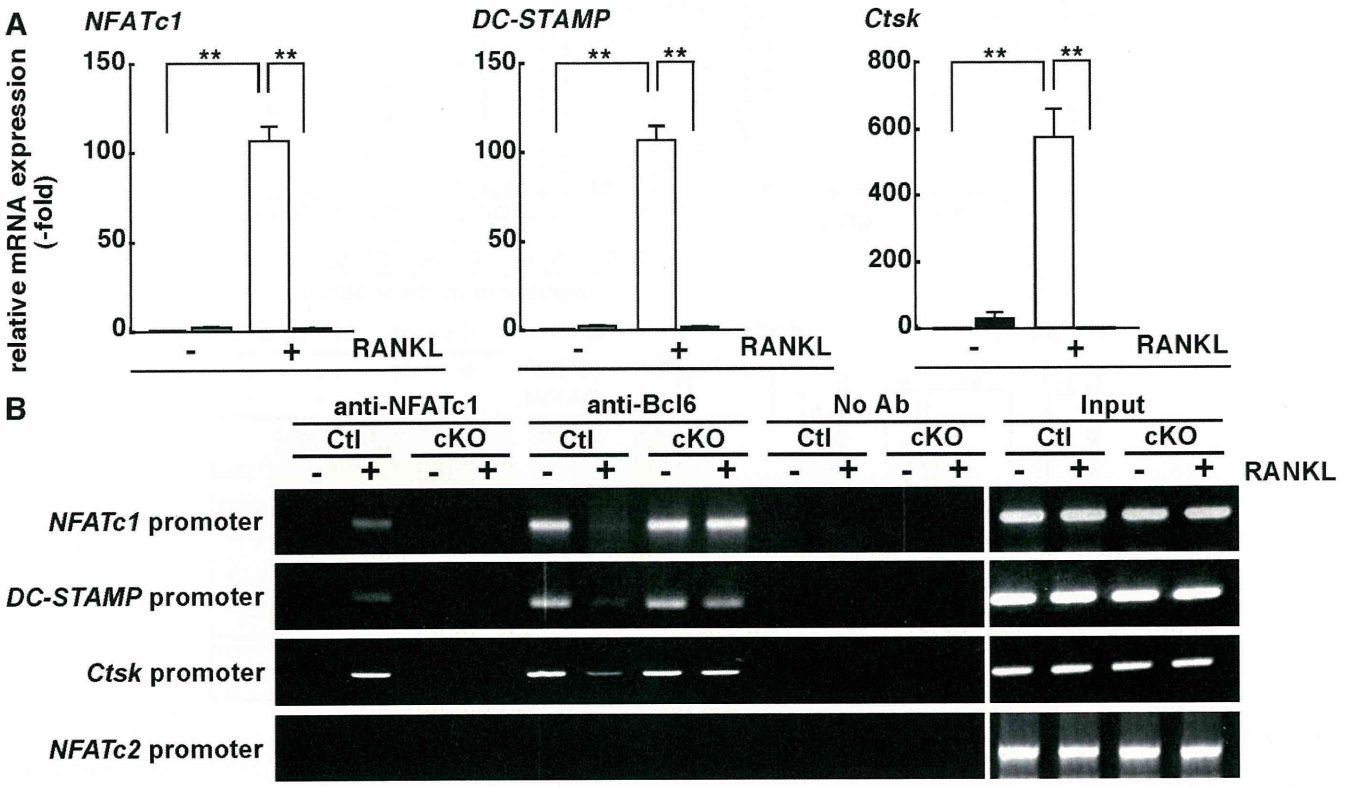

Figure 5. Bcl6 suppresses osteoclast differentiation. (A) Total RNA was prepared from control (white bars) or Blimp1 cKO (shaded bars) cells treated with (+) or without (−) RANKL, and the expression of the osteoclastic genes *NFATc1*, *DC-STAMP*, and *Ctsk* relative to *β-actin* was analyzed by a quantitative real-time PCR. Data are means ± SD of *osteoclastic genes*/*β-actin*. (**, $P < 0.001$; $n = 4$). (B) Recruitment of NFATc1 and Bcl6 to promoters of osteoclastic genes such as *NFATc1*, *DC-STAMP*, *Ctsk*, or a negative control gene *NFATc2* was analyzed by a ChIP assay. Representatives of at least four (A) or two (B) independent experiments are shown.

Published April 5, 2010

JEM

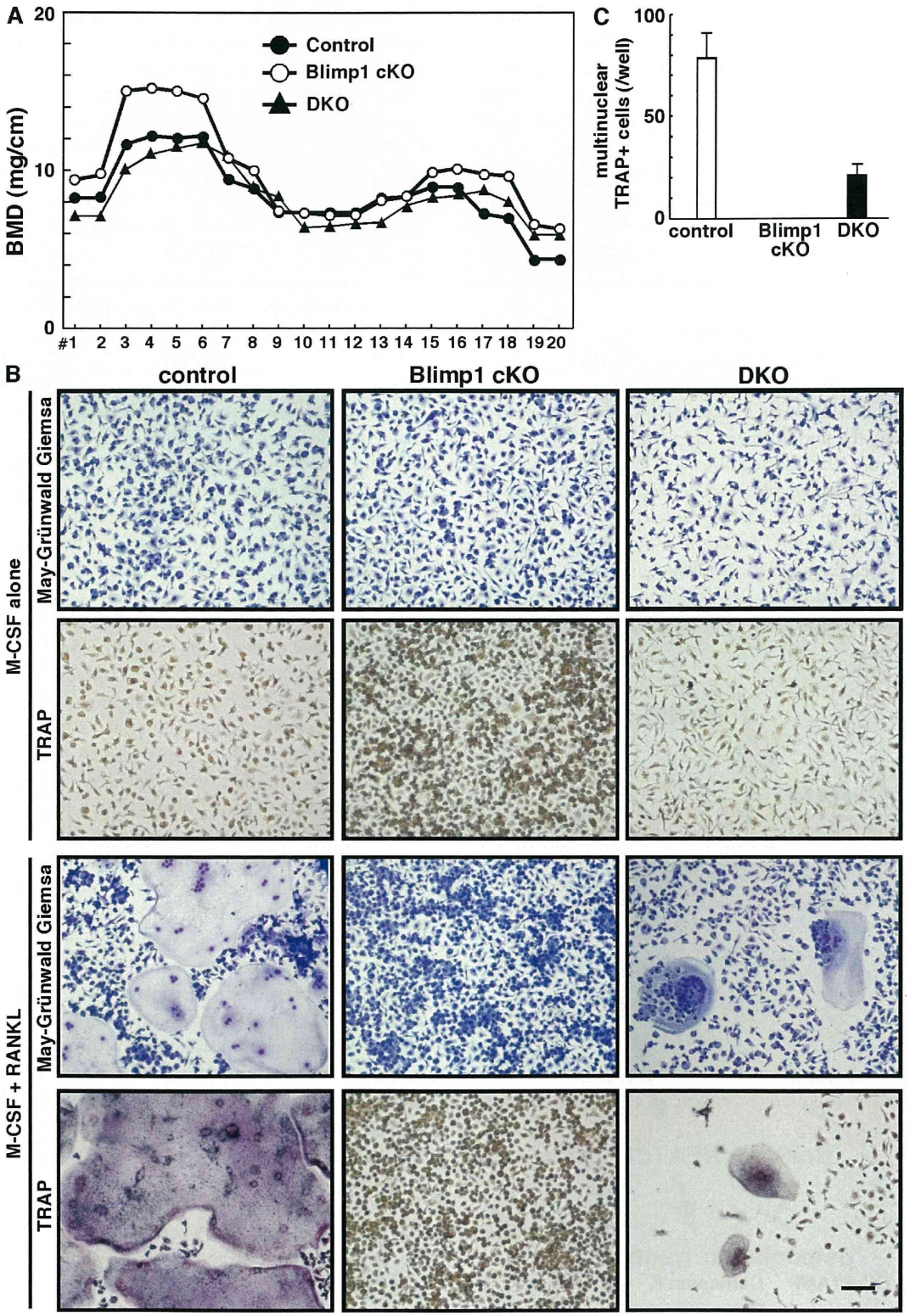

Figure 6. Bcl6 is a target of Blimp1 during osteoclastogenesis. (A) Bone mineral density (BMD) of equal longitudinal division of femurs of control (filled circles), Blimp1 cKO (open circles), and Blimp1 cKO/Bcl6 KO (DKO; filled triangles) mice. Data represent mean BMD ($n = 4$). (B and C) Osteoclast progenitor cells from control, Blimp1 cKO or DKO mice were cultured in the presence of M-CSF alone or M-CSF plus RANKL for 8 d. Cells were then subjected to May-Grünwald Giemsa and TRAP staining (B), and the number of TRAP-positive cells containing more than three nuclei was scored (C). Results are representative of three independent experiments. Bar, 100 µm.

Published April 5, 2010

of *Bcl6* expression caused by Blimp1 deficiency leads to osteoclastogenesis failure, as indicated by increased bone mass seen in a Blimp1 cKO model. Signals positively regulating NFATc1 in osteoclasts, such as TRAF6, c-Fos, ITAM-PLCγ-Ca^{2+} signals, Btk, and Tec (Takayanagi et al., 2002; Koga et al., 2004; Shinohara et al., 2008), have been characterized, and NFATc1 reportedly positively autoregulates in osteoclasts (Asagiri et al., 2005). However, factors modulating this activity have not been described. Our study characterizes such an axis of factors that serve as a molecular switch to control osteoclastogenesis and bone homeostasis after RANKL stimulation.

To date, the skeletal and immune systems have been shown to share common molecules to achieve homeostasis (Nakashima and Takayanagi, 2008). RANKL and RANK were originally identified in T cells and DCs (Anderson et al., 1997), respectively, and both are essential for osteoclastogenesis (Kong et al., 1999; Dougall et al., 1999). NFATc1 was identified in T cells and plays an essential role in osteoclast formation (Northrop et al., 1994; Asagiri et al., 2005). DC-STAMP plays a role in DC function and is required for cell–cell fusion of osteoclasts and macrophage giant cells (Yagi et al., 2005, 2007; Sawatani et al., 2008). Besides roles in immune system, Bcl6 has antiapoptotic and protooncogenic function

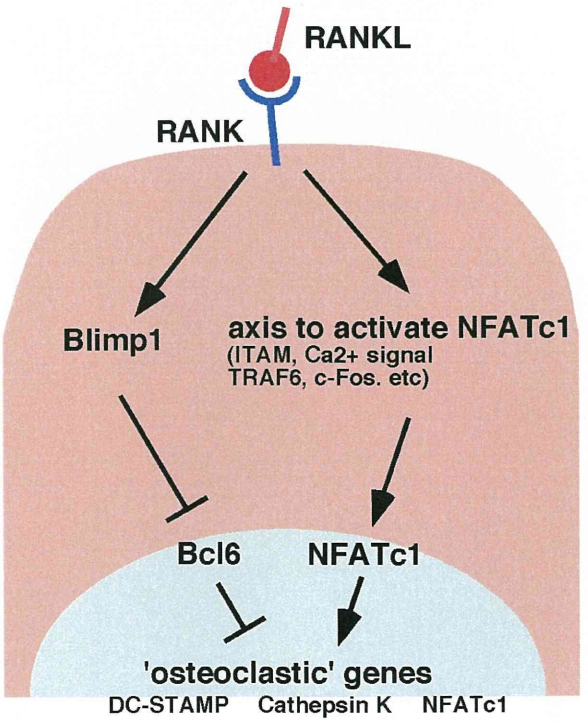

Figure 7. A schematic model of osteoclastogenesis regulated by the Blimp1–Bcl6–osteoclastic gene axis. RANKL–RANK interaction results in Blimp1 induction, leading to Bcl6 down-regulation and dissociation of Bcl6 from osteoclastic gene promoters, an event critical for osteoclastogenesis. NFATc1 activation is induced by various factors, such as ITAM, TRAF6, c-Fos, and Ca^{2+} signaling, which are also activated by RANKL.

(Baron et al., 2002; Ohno, 2006). Blimp1 also functions in specification of the germ cell lineage and acts as a tumor suppressor (Ohinata et al., 2005; John and Garrett-Sinha, 2009). Here, we show that Bcl6 and Blimp1, which are both implicated in B cell and T cell development (Turner et al., 1994; Fukuda et al., 1997; Dent et al., 1998; Kusam et al., 2003; Ichii et al., 2004; Kallies et al., 2006; Martins et al., 2006; Cimmino et al., 2008), have a novel function in regulating osteoclastogenesis and maintenance of bone homeostasis. It has been reported that Blimp1 represses Bcl6 (Cimmino et al., 2008) or that Blimp1 and Bcl6 regulate each other (Shapiro-Shelef and Calame, 2005). Blimp1 expression was reportedly inhibited by Bcl6 (Martins et al., 2006); however, we did not detect dysregulation of Blimp1 expression in Bcl6-deficient osteoclasts (unpublished data). Osteoclast-specific Blimp1/Bcl6 DKO mice exhibited increased osteoclastogenesis with decreased bone mass compared with Blimp1 cKO mice, indicating that Blimp1 regulates Bcl6 in osteoclasts. However, although Bcl6-deficient cells showed accelerated osteoclastogenesis compared with control cells, DKO cells showed decreased osteoclast differentiation compared with control cells, suggesting that Blimp1 regulates osteoclastogenesis through Bcl6 along with other target molecules. Blimp1 has multiple targets in lymphocytes and PGCs (Shaffer et al., 2002; Kurimoto et al., 2008), and thus it is possible that Blimp1 has multiple targets in osteoclasts as well. In osteoclasts, several negative regulators for osteoclastogenesis, such as *Id*, *Mafb*, and *Irf8*, have been identified (Lee et al., 2006; Kim et al., 2007; Zhao et al., 2009). Blimp1 may also target these molecules in osteoclasts to stimulate osteoclast differentiation. Further investigations are needed to clarify the molecular mechanisms of the regulation of osteoclastogenesis by Blimp1.

We used $Ctsk^{Cre/+}$ mice to establish osteoclast-specific Blimp1 cKO mice because $Ctsk^{Cre/+}$ mice have been used to generate osteoclast-specific KOs of factors such as the estrogen receptor and Bcl-XL (Nakamura et al., 2007; Iwasawa et al., 2009). Osteoclastogenesis, including *Ctsk* expression, has been evaluated in osteoclast-specific gene-targeted cells (Nakamura et al., 2007). *Blimp1* expression is induced earlier than *Ctsk* (Fig. 3 A), and osteoclastogenesis is inhibited in Blimp1 cKO cells, suggesting that continuous Blimp1 expression is required for full osteoclast differentiation under control of RANKL. Blimp1 is also known to be induced by BMP4 and LIF in PGCs, where it functions as a transcriptional repressor (Ohinata et al., 2009). In osteoclasts, Blimp1 is induced by RANKL and acts to repress Bcl6. Thus, signaling regulating Blimp1 expression differs between PGCs and osteoclasts.

Bone homeostasis requires a delicate balance between osteoclastic and osteoblastic activities. A decline in bone volume is closely related to up-regulation of osteoclast activity, and thus osteoclasts could be targeted therapeutically to treat skeletal disorders such as osteoporosis and destructive bone metastasis. FK506, a specific inhibitor of calcineurin-NFATs, inhibits osteoclastogenesis, but does not increase bone mass, as FK506 also inhibits bone formation (Koga et al., 2005). Thus, additional factors that could negatively regulate osteoclast